COMPDYN 2009
ECCOMAS Thematic Conference on
Computational Methods in Structural Dynamics and Earthquake Engineering
M. Papadrakakis, N.D. Lagaros, M. Fragiadakis (eds.)
Rhodes, Greece, 22–24 June 2009

THE EFFECT OF DIAPHRAGM WAVE PROPAGATION ON THE ANALYSIS OF POUNDING STRUCTURES

Gregory L. Cole[1], Rajesh P. Dhakal[2], Athol J. Carr[2], and Des K. Bull[2]

[1] University of Canterbury
Private Bag 4800
Christchurch 8140
e-mail: glc24@student.canterbury.ac.nz

[2] University of Canterbury
Rajesh.Dhakal@canterbury.ac.nz
Athol.Carr@canterbury.ac.nz
Des.Bull@canterbury.ac.nz

Keywords: Pounding, Wave Propagation, Distributed Mass, Collision Element, Building, Impact.

Abstract. *Building pounding is frequently observed during earthquakes in regions of dense urban populations, with damage levels ranging from cosmetic to catastrophic for buildings with insufficient separation. While the numerical modeling of pounding has significantly progressed in recent years, significant uncertainty still remains in many collision properties. The collision force itself is highly dependent on the stiffness of the so called 'collision element', yet this stiffness is not well characterized in the existing literature.*

This paper identifies building pounding as the collision of two distributed masses and subsequently analyses the collision in terms of the one dimensional wave equation. Collision properties are derived from wave theory and numerically verified, building on the work of previous researchers [1]. An 'instant wave' method is proposed as a distributed mass equivalent to stereo mechanics.

Numerical approximations of distributed masses are assessed in terms of displacement response. Two building configurations are subjected to 10 second excitations with 5 % modal damping. The collision element stiffness in lumped mass models is also investigated to determine the most accurate response. It is found that at least three nodal masses connected by axial spring elements should be used to represent each diaphragm in order to provide consistently accurate displacement results. The contact element stiffness should be calculated with $\gamma = 1$ and the element stiffness of the stiffer diaphragm should be used in this calculation.

1 INTRODUCTION

Seismic pounding occurs when earthquake excitation causes adjacent buildings to collide. The phenomenon has been widely researched since pounding's reported devastation in the 1985 Mexico City Earthquake [2], although studies had also been published prior to this event. Many researchers have investigated pounding with time history simulation and typically created a numerical model similar to Figure 1. Each node point represents a floor of a building which are connected to the adjacent building through a 'collision element'. The collision element exhibits zero stiffness until the building separation is closed whereupon a very large stiffness is defined. Plasticity can also be added to the collision by including a viscous damper in parallel. Early studies found building displacement response to be insensitive to the collision stiffness [3, 4]. Various alternative collision elements have also been developed for building pounding, however all are tested assuming the diaphragms act as lumped masses [5-7]. The collision element can be avoided entirely by instead applying the laws of stereo mechanics [8]. When a collision occurs, the post collision velocities are calculated by conservation of momentum assuming both diaphragms are lumped masses. The simulation then continues with the updated velocities. Stereo mechanics and collision elements produce similar post collision velocities. Stereo mechanics is not commonly used since it is not easily incorporated into modern numerical tools.

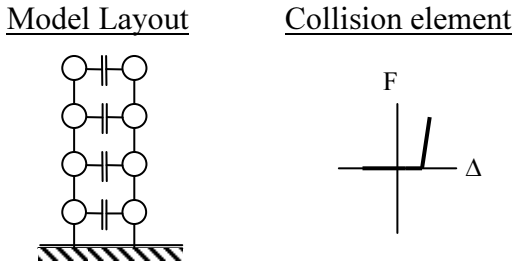

Figure 1: Typical numerical model of two impacting buildings

The assumption that a diaphragm is appropriately modeled as a lumped mass has not been challenged in building pounding literature. Classical physics demonstrates that distributed masses and lumped masses yield different collision force profiles and collision durations [8]. Watanabe and Kawashima [1] investigated the collision of distributed masses in relation to bridge decks. They discretised two distributed masses into a series of spring elements with lumped masses at the nodes, as shown in Figure 2. Diaphragm parameters were chosen such that both building's element stiffnesses (k_E) were the same. Single collisions were investigated with 5, 10 and 20 elements in each diaphragm. It was demonstrated that distributed masses cause different post collision velocities when compared to equivalent lumped mass models if the length of the two diaphragms differ. It was further shown that when two distributed mass diaphragms collide, the most accurate stiffness for the collision element is found when $\gamma = 1$, where γ is defined as

$$k_C = \gamma k_E = \gamma \frac{nEA}{L} \tag{1}$$

where k_C is the collision stiffness, k_E is the individual element stiffness and L, E A and n are the diaphragm's length, modulus of elasticity, area, and number of elements respectively.

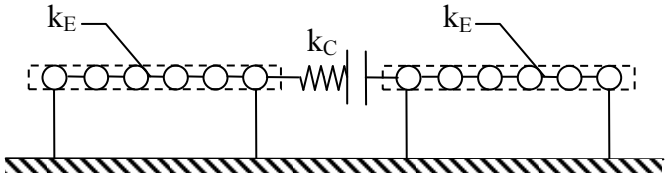

Figure 2: Discretised diaphragms with contact element

This paper extends the work of Watanabe and Kawashima [1] to consider multiple collisions between three different configurations of adjacent buildings with distributed masses. Wave theory is extended and an 'instant wave' model is proposed. Results are analyzed to determine whether the lumped mass assumption causes significant loss of accuracy in the displacement response of the structure. The characteristics of the impact force are also investigated in the context of distributed mass collisions. Furthermore, the paper extends the analogy of Equation 1 to lumped mass models (zero element diaphragms) to provide guidance to future researchers when selecting the collision element stiffness.

2 WAVE THEORY

Impact wave theory has been published previously with varying degrees of detail. Goldsmith's classical physics text [8] contains an alternate derivation using the D'Alembert solution. Collision with a distributed mass is most appropriately analyzed by the one dimensional wave equation.

$$\frac{\partial^2 u(x,t)}{\partial t^2} = c^2 \frac{\partial^2 u(x,t)}{\partial x^2} \qquad where \;\; c^2 = \frac{E}{\rho} \tag{2}$$

where c, E and ρ are the distributed mass's wave velocity, modulus of elasticity and material density of the object, respectively. u(x,t) is a generic parameter describing the displacement of a point x in the mass at a time t and is defined as zero for all points on the mass at time t = 0. In other words u is a measure of how much movement occurs at each point relative to its position immediately before an impact. For example, if a distributed mass travelled at a uniform velocity v (without any internal strain) it would be represented as u(x,t) = vt, without any dependence on x. Alternatively, if a uniform compression strain was applied across the mass where time t = 0 seconds refers to the unstressed state, the steady state solution is u(x,t) = δx/L where δ is the overall compression deformation.

2.1 Collision of a single distributed mass with a rigid wall

Consider the collision of a distributed mass moving at a constant velocity and an infinitely rigid wall (Figure 3).

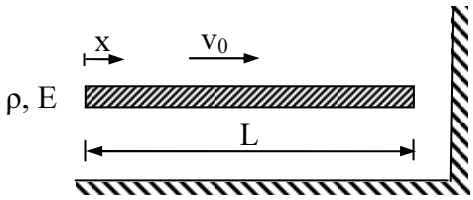

Figure 3: Collision of a distributed mass and a rigid object

The Partial Differential Equation (PDE) describes the motion of the mass for the duration of the collision, and requires two boundary conditions and two initial conditions for its solution. These are the following:

1. The strain is zero at x = 0 (since no stress can be transmitted from the end of the distributed mass to the air);
2. The displacement at the collision end of the mass is zero;
3. At t = 0, the velocity throughout the mass is a constant v_0; and
4. At t = 0, the displacement throughout the mass is zero.

The conditions are expressed mathematically as

$$\begin{aligned} \frac{\partial u(0,t)}{\partial x} &= 0 & u(L,t) &= 0 \\ \frac{\partial u(x,0)}{\partial t} &= \mathrm{v}_0 & u(x,0) &= 0 \end{aligned} \tag{3}$$

The second and third conditions are technically contradictory, since the second condition implies the impact has already started, which means the velocity at x = L must be zero. This phenomenon is well recognized in the solution of PDEs and can be ignored as it does not adversely affect the final solution. The PDE (Equation 2) is solved by separation of variables;

$$u(x,t) = \sum_{n=1}^{\infty} \frac{8\mathrm{v}_0 L(-1)^{n+1}}{(2n-1)^2 \pi^2 c} \cos\left(\frac{(2n-1)\pi}{2L} x\right) \sin\left(\frac{(2n-1)\pi}{2L} ct\right) \tag{4}$$

The solution can be normalised as follows

$$\begin{aligned} \mathrm{T} &= \frac{c}{L} t & \mathrm{X} &= \frac{x}{L} \\ u(x,t) &= \frac{\mathrm{v}_0 L}{c} U(\mathrm{X},\mathrm{T}) \\ \mathrm{v}(x,t) &= \frac{\delta u(x,t)}{\delta t} = \mathrm{v}_0 \mathrm{V}(\mathrm{X},\mathrm{T}) \\ \mathrm{a}(x,t) &= \frac{\delta^2 u(x,t)}{\delta t^2} = \frac{\mathrm{v}_0 c}{L} \mathrm{A}(\mathrm{X},\mathrm{T}) \\ f(x,t) &= E \frac{\delta u(x,t)}{\delta x} = \frac{\mathrm{E}\mathrm{v}_0}{c} \mathrm{F}(\mathrm{X},\mathrm{T}) \end{aligned} \tag{5}$$

U: 0 → 1, V: -1 → 1, A: - ∞ → 0 and F: -1 → 0

where u, v, a and f are the distributed mass's displacement, velocity, acceleration and stress respectively. The dimensionless numbers U, V, A and F are mathematical sums of infinite series. Figure 4a illustrates the physical reality of Equations 4 and 5. Time is normalized by the time the stress wave takes to travel the length of the mass. The figure shows a stress wave propagate through the diaphragm, reflect off the free end and then negate itself such that when the collision is completed no oscillation remains in the mass. Note the instant changes in velocity cause an instantaneous infinite acceleration at that point. In reality this acceleration is finite as a purely clean collision cannot be realistically imposed.

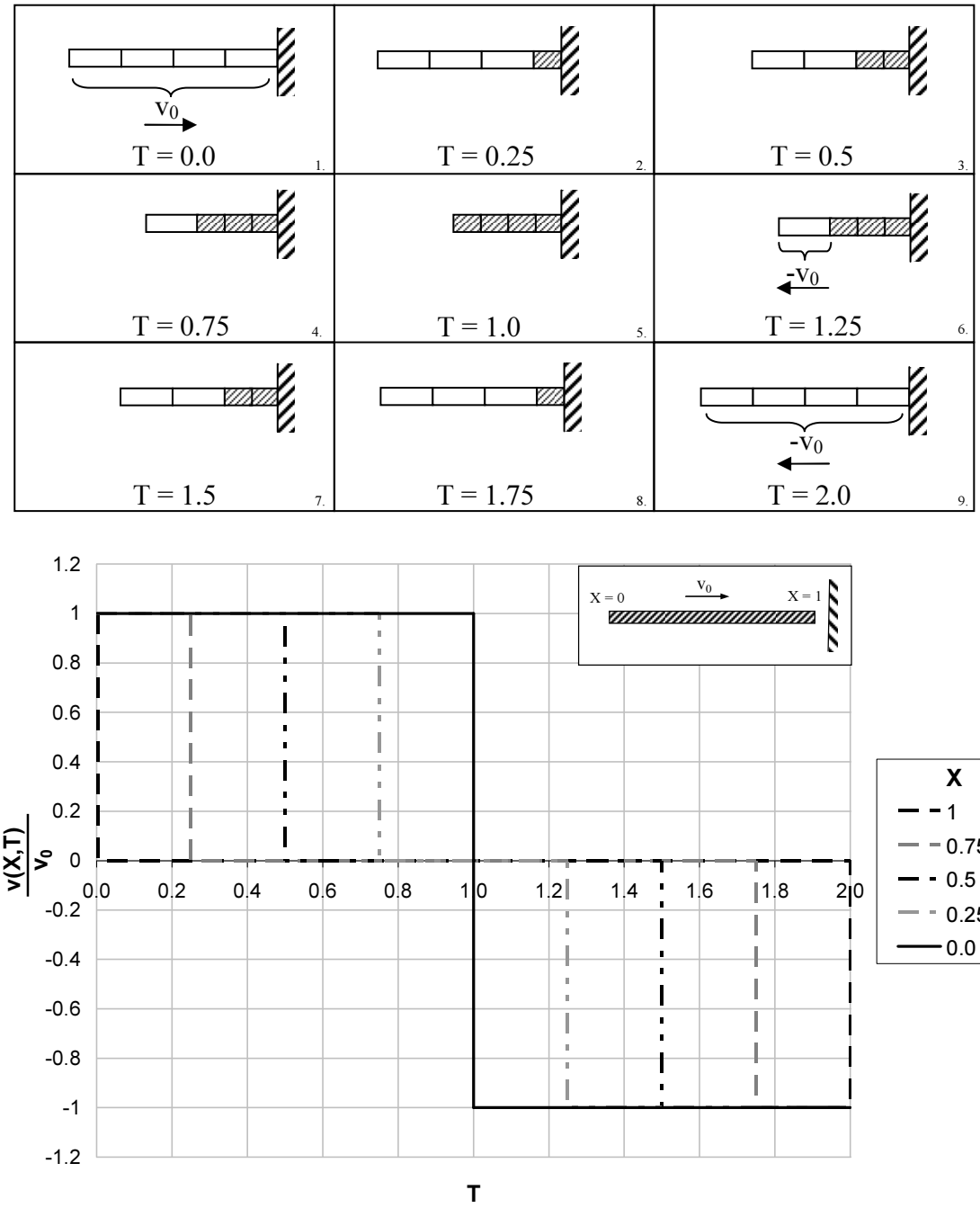

Figure 4a: Instants in a single distributed mass colliding with a rigid barrier (hashed areas denote compression) and 4b: Dimensionless velocity profile.

Equation 4 describes the nature of the collision only until T = 2.0 as shown in Figure 4a. After this point, the mass moves away from the rigid wall, changing the second boundary condition. The collision duration can be found by inspection of the final instant in Figure 4a. At the end of the collision, all points are in the same location as they were before the collision started, with an equal and opposite velocity. Mathematically, the collision duration can be found by determining when all terms in the infinite sum equal zero for all x. This occurs when all sine terms are zero, which first occurs at (ignoring the trivial solution t = 0);

$$\frac{(2n-1)\pi}{2L} cT_{col} = \pi$$
$$T_{col} = \frac{2L}{c} = 2L\sqrt{\frac{\rho}{E}} \tag{6}$$

The term T_{col} is the axial period of the distributed mass (as n = 1 is the fundamental mode). Since it also describes the duration of the collision, it is hereafter referred to as the 'natural collision period'. As seen in Equation 5, all collision properties are directly proportional to the initial velocity. The collision velocity can be completely described by the dimensionless chart shown in Figure 4b. The five values of X correspond to the five vertical lines in the mass shown in Figure 4a. No velocity is lost during the collision due to conservation of momentum.

2.2 Collision of two distributed masses

When two distributed masses traveling at constant velocity impact as shown in Figure 5, the resulting collision is described by two Partial Differential Equations, each requiring two boundary and two initial conditions.

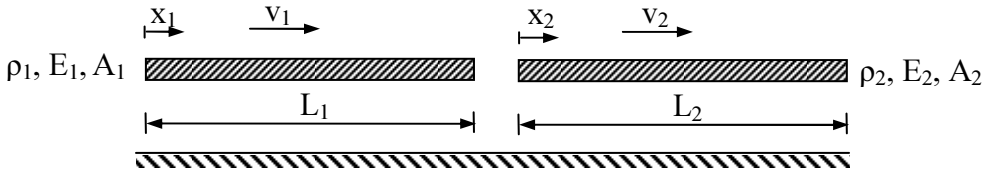

Figure 5: Collision of two distributed masses

The boundary conditions remain the same for the free ends of each mass, however the behavior of the collision interface must be mathematically defined. Upon collision, both masses respond with a shock wave that travels their respective lengths, reflects and travels back to the collision interface. While these waves travel, the collision interface itself moves with at a constant velocity, v_c. The collision interface velocity is determined by the initial velocities and the rates of compression of both masses. The collision of either mass can be alternatively visualized as a single distributed mass colliding with a rigid boundary moving at velocity v_c. To determine this velocity, consider the free body diagram consisting of an infinitesimal part of each mass either side of the collision interface. Refer to the second instant in Figure 6a, in order for the interface to move at constant velocity the internal force in each mass must be equal and opposite. The internal force in each mass is calculated by multiplying the stress displayed in Equation 5 by its corresponding area. The velocity v_0 is now equal to the initial diaphragm velocity less the collision interface velocity;

$$\frac{A_1E_1(v_1 - v_c)}{c_1} F_1(1, T_1) + \frac{A_2E_2(v_2 - v_c)}{c_2} F_2(0, T_2) = 0$$
$$F_1(1, T_1) = F_2(0, T_2) = \sum_{n=1}^{\infty} \frac{4(-1)^{n+1}}{(2n-1)\pi} \sin\left(\frac{(2n-1)\pi}{2}\right) \sin\left(\frac{(2n-1)\pi}{2} T_{1,2}\right) = 1.0 \tag{7}$$
$$\therefore\ v_c = \frac{A_1\sqrt{\rho_1E_1}\,v_1 + A_2\sqrt{\rho_2E_2}\,v_2}{A_1\sqrt{\rho_1E_1} + A_2\sqrt{\rho_2E_2}}$$

Note that $F_1(1,T_1) = F_2(0,T_2) = 1.0$ is valid only for the duration of the collision.

As v_c is now defined, each distributed mass can be analyzed in isolation. The complete solution for a mass 1 is;

$$u_1(x,t) = v_c t + \sum_{n=1}^{\infty} \frac{8(v_1 - v_c)(-1)^{n+1} L_1}{(2n-1)^2 \pi^2 c_1} \cos\left(\frac{(2n-1)\pi}{2L_1} x\right) \sin\left(\frac{(2n-1)\pi}{2L_1} c_1 t\right) \quad (8)$$

The corresponding solution for mass 2 is similar, but requires (L – x) instead of just x since the shock wave propagates in the opposite direction. Setting $v_c = 0$ m/s provides Equation 4. The primary difference between Equations 8 and 4 is the term $v_c t$, which allows both masses to move during the collision. Figure 6a illustrates the result where $c_1 > c_2$. The collision occurs in a similar manner to Figure 4a, and includes the overall translation caused by $v_c t$. Equation 8 is also only valid until the two diaphragms separate. This occurs when time reaches the first of the two masses' natural collision periods. Once this point is reached, the mass with the shorter period moves away while the other mass internally oscillates. This is due the incomplete reflection of the shock wave.

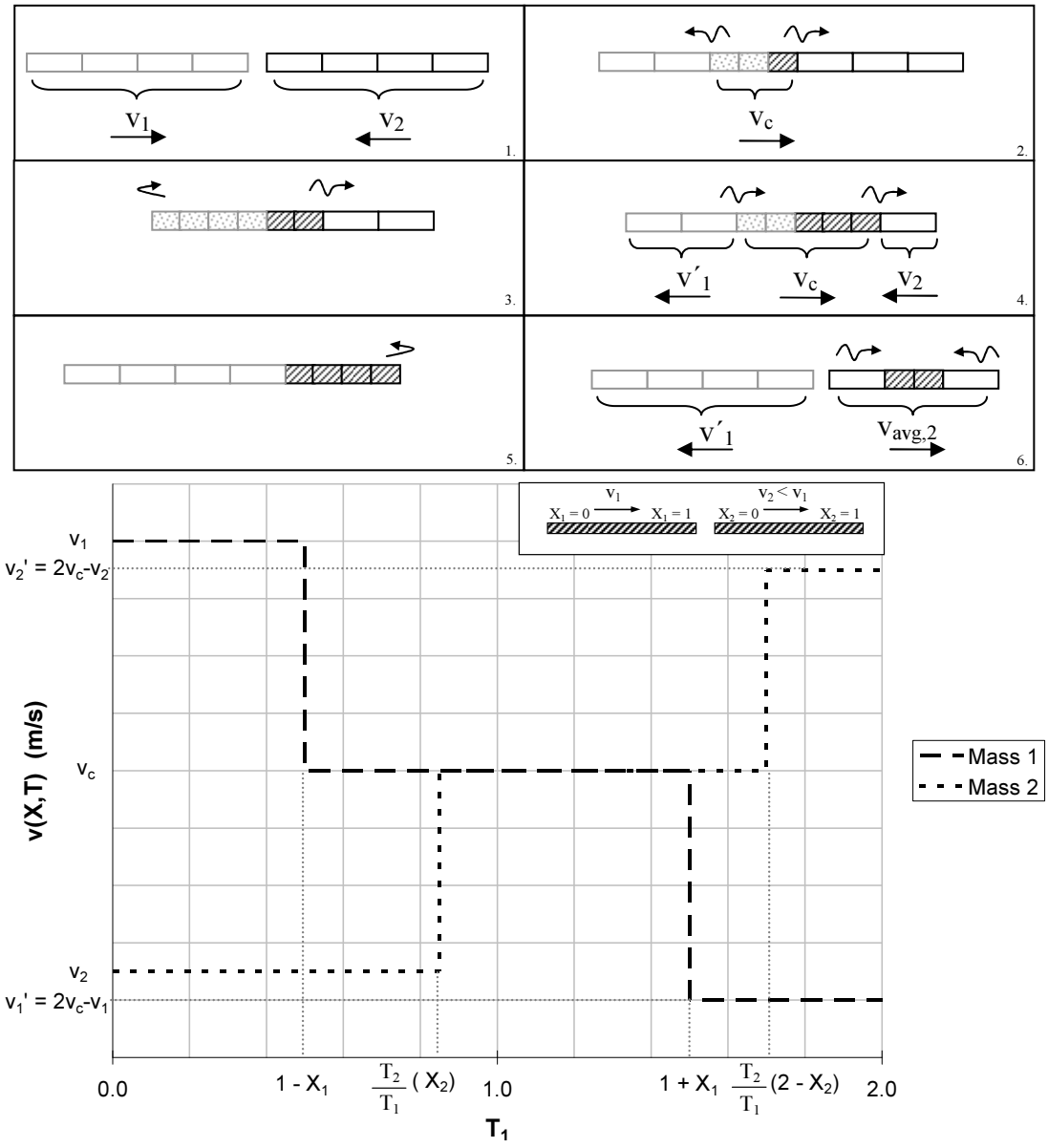

Figure 6a: Instants in a two distributed mass collision and 6b: Dimensionless velocity profile ($T_1 < T_2$).

Unlike the single mass case, dimensionless profiles no longer fall onto a single curve, but depend on v_i/v_c where i is the mass under consideration. The velocity profiles are instead expressed as a generalized plot as shown in Figure 6b. Particles in either mass continue to move at their initial velocity until the wave passes them, after which these particles immediately start moving at the collision interface velocity. The particle velocity changes again when the reflected wave passes the same location and moves at the post collision velocity. For example, a point half way along mass 1 will travel at its initial velocity for one quarter of the collision, at which point it suddenly starts to travel at velocity v_c. This velocity changes again three quarters of the way through the collision to mass 1's post collision velocity. The behavior of mass 2's particles is similar but must be scaled in time by its own natural collision period. As shown in Figure 6b, if the properties and initial velocities of both masses are known, then the post collision velocity of the i^{th} mass is;

$$v_i' = 2v_C - v_i \qquad \textit{(i = 1, 2)} \quad (9)$$

The collision force can be found by inspecting the strain at the collision interface. The strain is in turn found by differentiating Equation 8 with respect to x. Throughout the collision the force at the interface holds a constant value of magnitude;

$$F_{Col} = \frac{A_i E_i (v_i - v_c)}{c_i} \qquad \textit{(i = 1, 2)} \quad (10)$$

The sixth instant of Figure 6a shows the mass with the longer collision period oscillating after the collision has finished. This behavior is not displayed in the theoretical profile as it requires a change in collision interface boundary condition. Such behavior also changes the mass's post collision velocity since more momentum transfer would occur if the other mass was still in contact. Since the collision force is known to be constant during the collision, the momentum (impulse) lost from the longer mass during the transfer process is directly proportional to the time lost from its collision period. The post collision velocity can therefore be determined by linearly interpolating between the mass's initial velocity, and its expected final velocity assuming full contact throughout the duration of the collision.

$$v_{avg,2} = \frac{T_{Col,1}}{T_{Col,2}} v_2' + \left(1 - \frac{T_{Col,1}}{T_{Col,2}}\right) v_2 \qquad (11)$$

where $T_{Col,1}$ and $T_{Col,2}$ are defined by Equation 6 and $T_{Col,1} < T_{Col,2}$

2.3 Theory limitations when modeling building diaphragms

In order for the above theory to completely describe two pounding diaphragms, four important assumptions are necessary;

1. Both diaphragms are assumed to have uniform seismic mass and floor stiffness across their length. Any diaphragm penetrations are assumed to have negligible influence;
2. Any collision occurs uniformly across the entire collision interface, no local geometric irregularities are accounted for. No torsional effects are modeled;
3. The ratio of diaphragm stiffness to column interstorey stiffness is sufficiently high that column stiffness can be ignored. That is, the column stiffnesses do not affect the behavior of the collision; and
4. No collision damping occurs (that is, the collision is elastic with a coefficient of restitution of 1.0).

In reality, none of these four assumptions are strictly true in any building. However, despite these simplifying assumptions the theory is still physically more accurate than the lumped mass model. The forth assumption is perhaps the most contestable. Researchers typically use a coefficient of restitution in the range of 0.4 to 0.75 [9] for lumped mass models. Whether a coefficient of restitution or an alternate method of impact reduction is appropriate is a matter for further research.

3 MODELING POUNDING AS INSTANTANEOUS COLLISIONS

Stereo mechanics has been used by previous researchers to modeling pounding [10]. Stereo mechanics provides identical post collision velocities as a lumped mass diaphragm model provided that three conditions are met:

1. No other external load is applied during the collision;
2. Any collision damping has been calibrated with the coefficient of restitution in stereo mechanics [11]; and
3. There is no acceleration in either diaphragm at the time of impact.

With these conditions, identical velocities occur because the lumped mass contains the same assumptions as stereo mechanics theory. Thus stereo mechanics is the 'instant collision' equivalent of the lumped mass diaphragm. The post collision velocity obtained by the wave equation can be directly compared to that of stereo mechanics by substituting for the diaphragm mass and axial stiffness, m and k, into Equations 7 & 9. After rearranging present the expression in a form similar to stereo mechanics, one can obtain;

$$v_1' = v_1 - 2\frac{1}{1+\sqrt{\frac{m_1 k_1}{m_2 k_2}}}(v_1 - v_2) \tag{12a}$$

Comparing it with the standard stereo mechanics [8];

$$v_1' = v_1 - 2\frac{1}{1+\frac{m_1}{m_2}}(v_1 - v_2) \tag{12b}$$

A generalized expression can be written as;

$$v_1' = v_1 - 2\alpha_1(v_1 - v_2) \tag{12c}$$

In the above equations, post collision velocity of mass 2 can be found by swapping the subscripts 1 and 2. Inspection of Equation 12 shows that the wave equation only produces the same post collision velocities when the diaphragm stiffness ratio is equal to the mass stiffness ratio. This only occurs when $T_{Col,1} = T_{Col,2.}$ Note that the sum of α_1 and α_2 is always equal to 1.0. Figure 7 illustrates the likely range of α for the two methods. Variation in α can be as large as 0.4. While greater values are technically possible, they are unlikely to be found in common pounding scenarios.

The degree to which α affects the post collision velocity, in turn, depends on the ratio of the two diaphragm velocities. This is illustrated in Figure 8 which plots Equation 12c a normalized. A change in the value of α affects the post collision velocity more when there are larger relative velocities. The post collision velocity is independent of α when $v_1 = v_2$, however this is trivial since no collision can occur while both objects move at the same velocity.

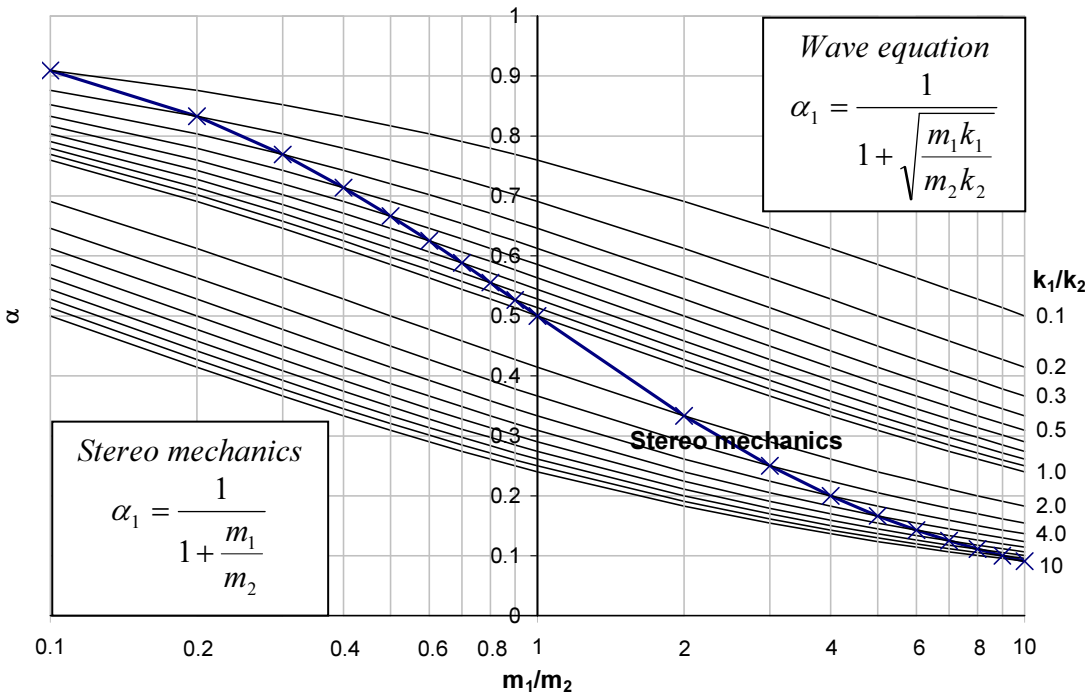

Figure 7: Effect of diaphragm stiffness ratio on α

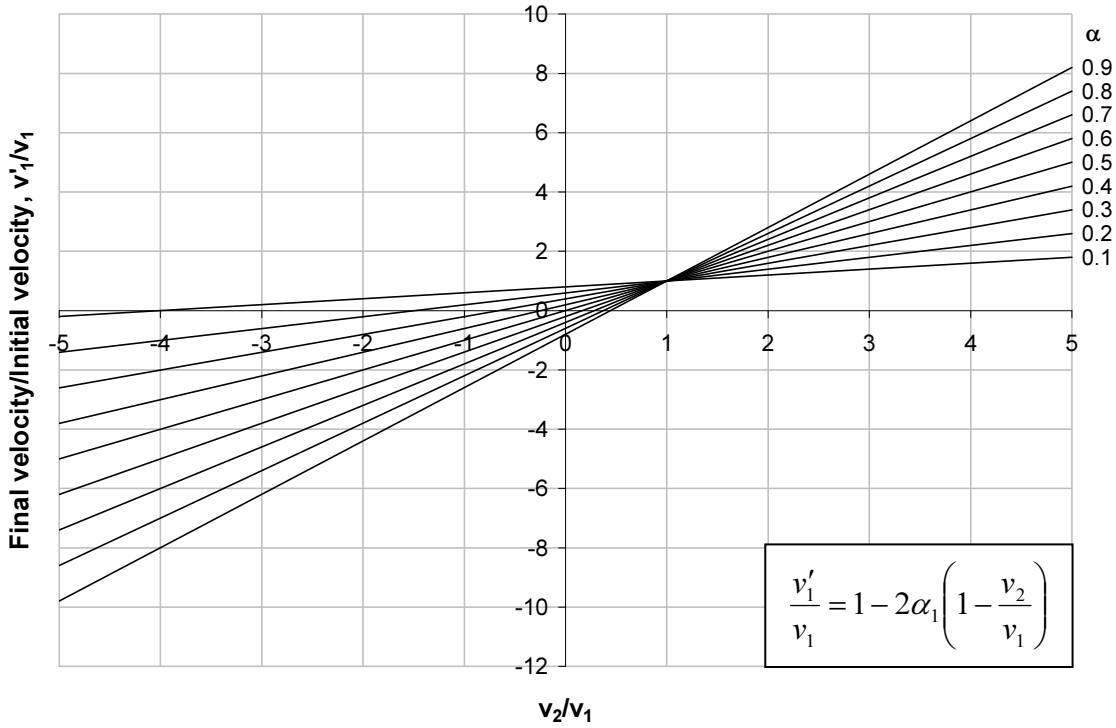

Figure 8: Influence of α on post collision velocity

3.1 The 'Instant Wave' method

Incorporating the effects of Equations 11 and 12a, a distributed mass instantaneous collision method can be proposed for use in numerical simulation of pounding. The underlying principles of this method are;

1. At any time when a collision occurs, post collision velocities are determined for each diaphragm by Equation 12a.
2. The velocity of the diaphragm with the longer collision period is modified by Equation 11.
3. Numerical simulation continues with the updated post collision velocities.

This process has been termed the 'instant wave' method. The effects of modeling the diaphragm as a distributed mass can therefore be examined by comparison of stereo mechanics and the instant wave equation.

The instant wave method presents new difficulties. The stereo mechanics approach necessarily assumes an instantaneous collision. This assumption is also used in the distributed mass formulation, yet for a distributed mass the collision duration is known. Alternatively some time lapse could be incorporated into the algorithm before imposing the change in velocity. However, this presents further problems in terms of the displacement history during the collision itself and how any further external excitation affects the outcome. The most important drawback is the implementation of instantaneous models in modern software packages. Since the accelerations are ignored during a collision, any numerical software that uses the acceleration from the previous time step as an input cannot be used without modification.

Important advantages also exist over the popular contact spring approach. A significantly larger time step can be used as intricate modeling of the diaphragm itself is not required. Computation takes seconds rather than minutes or hours for the larger models. Similarly, only a single node per diaphragm is required. Furthermore, the definition of a gap element is unnecessary, avoiding the need to calibrate any collision element stiffness. If an element representing the diaphragm is to be used in an analysis of this type, the nodes at either end should be slaved so the diaphragm's interaction is not modeled twice. While this method is not common for most modern analysis, it can serve as an informative tool to provide insight into the mechanics governing pounding.

To investigate the difference caused by the instant wave model, two Single Degree Of Freedom (SDOF) elastic structures were subjected to an excitation resulting in building pounding. Analysis was undertaken using both stereo mechanics and the instant wave equations. Buildings were separated by only 2 mm to ensure many collisions occurred. Over 50 collisions occurred during the 30 second record. Analyses were undertaken using a recurrence formula which is valid for elastic structures [12]. At the end of each time step, the building displacements are checked to see whether contact occurs. If contact does occur, the building velocities are updated according to the specific method. Both simulations were subject to 5 % modal damping.

Figure 9 displays the displacement history for both methods while Figure 10 compares the predicted post collision velocities. Using velocity data just prior to each collision from the instant wave method, Figure 10 compares post collision velocities immediately after each collision. Figure 10 shows consistently more positive (or less negative) post collision velocities predicted by the instant wave method. This behavior can be explained in terms of Figure 8 by comparison of the values of α used by the two methods. Figure 8 can be separated into two categories. If $v_2/v_1 < 1$, v_1 must be positive to cause a collision and a smaller value of α results in a less negative final velocity. Conversely, if $v_2/v_1 < 1$, v_1 must be negative to cause a collision. Therefore, even through a smaller value of α results in a less positive v'_1/v_1, the

negative value of the denominator causes v'_1 to be more positive. Equation 11 does not affect building 1 as it has the shorter natural collision period.

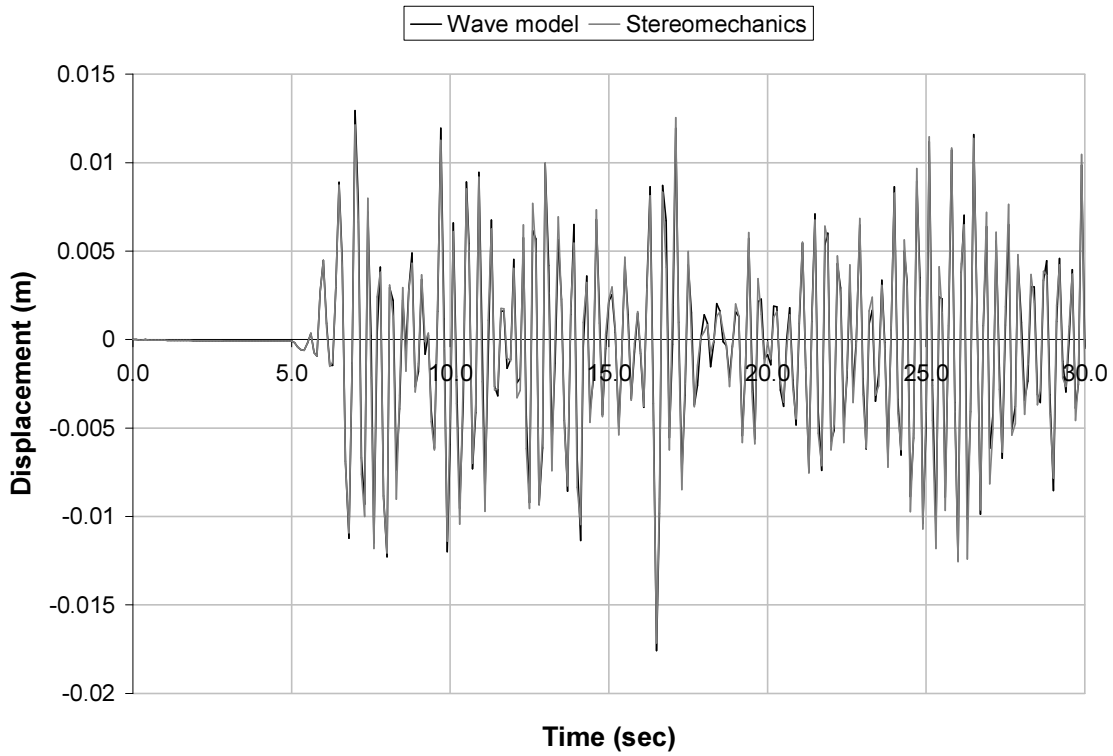

Figure 9: Building 1 displacement response
(T_1 = 0.4 sec, T_2 = 0.35 sec, m_1 = 163 Ton, m_2 = 306 Ton, k_1/k_2 = 2.5, m_1/m_2 = 0.53 T_{Col1}/T_{Col2}= 0.46)

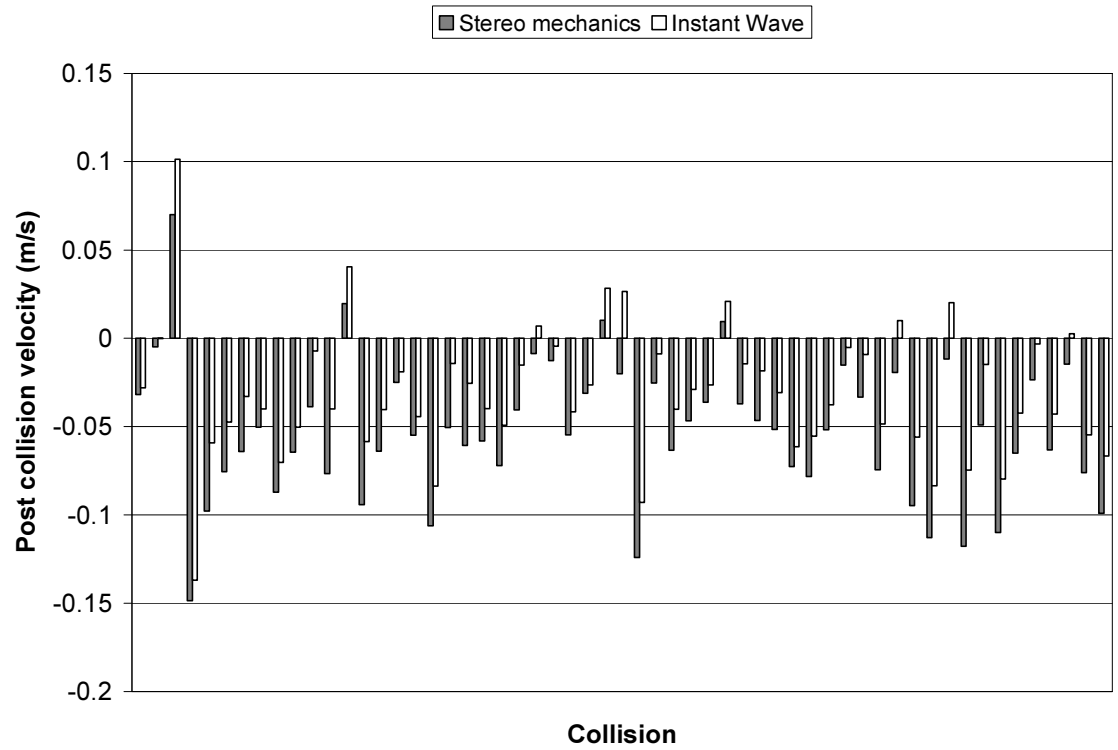

Figure 10: Building 1 post collision velocities (Stereo α_1 = 0.652, Instant Wave α_1 = 0.464)

Given the results of Figure 10, Figure 9 show surprisingly little difference in the displacement results. This is a general trend noted when comparing a number of different building configurations. The behavior might be attributable to the earthquake response overriding the actions resulting from pounding. Figures 9 and 10 show that the two methods have a marked effect on individual collision properties but significantly less effect on the overall displacement response.

3.2 Indicators of wave equation influence

Equations 11 and 12 highlight the two parameters that determine how different the post collision velocities are between the two methods. Post collision velocities diverge when the collision period ratio increases, or when the difference between stereo mechanics α and instant wave α increases. Finally, the discrepancy will also depend on the relative velocity of the two diaphragms at the onset of collision. Therefore the significance of wave propagation effects can be qualitatively assessed solely on these values.

3.3 Key collision equations

Other key parameters can also be simply defined by substituting for diaphragm mass and stiffness;

$$T_{Col} = 2\sqrt{\frac{m}{k}}$$
$$v_c = \frac{\sqrt{m_1 k_1}\,\mathrm{v}_1 + \sqrt{m_2 k_2}\,\mathrm{v}_2}{\sqrt{m_1 k_1} + \sqrt{m_2 k_2}} \tag{13}$$

Substitution for diaphragm mass and stiffness into Equation 10 provides the collision force;

$$F_{Col} = \frac{\mathrm{v}_1 - \mathrm{v}_2}{\frac{1}{\sqrt{m_1 k_1}} + \frac{1}{\sqrt{m_2 k_2}}} \tag{14}$$

The collision force cannot be calculated in stereo mechanics as the collision duration is assumed to be instantaneous. This presents an important advantage of the instant wave method, and as shown in later sections, any distributed diaphragm configuration. In the authors' knowledge, this is the first analytical method for calculating a contact force to be presented in pounding literature.

4 NUMERICAL MODELLING OF DISTRIBUTED MASS DIAPHRAGMS

Numerical modeling of a diaphragm distributed mass system requires a descretisation approximation. The diaphragm is modeled by connecting multiple nodal masses with axial springs. Two elastic SDOF buildings are first investigated to determine general behavior of the numerical approximation. The following two sections then investigate two building configurations for three different excitations. All analyses were undertaken using Ruaumoko 2D, an inelastic time history software package developed at the University of Canterbury [13]. Equivalent viscous damping was set as 5 % in all modes.

4.1 Elastic single storey pounding

The two elastic single storey structures separated by a 5 mm gap were subjected to a five second extract from El Centro, which resulted in pounding. Diaphragms were descretised as described in Figure 2, with masses assigned to each node according to their tributary length. Analyses were undertaken for n = 0, 1, 5, 10, 20 and 100 elements per diaphragm. A 500 element case was attempted but could not be analyzed as the computation time was in excess of a month. For the zero element (lumped mass) case three values of γ were investigated, γ = 0.1, 1, 10 where γ is defined in Equation 1. Note that γ was defined with respect to the stiffer of the two building diaphragms. As the system was entirely elastic, stereo mechanics and instant wave results can also be directly compared. Assuming the 100 node case as the accurate solution, Figure 11 shows the percentile error associated with the predicted maximum or minimum displacement values from the different discretisation and modeling approaches.

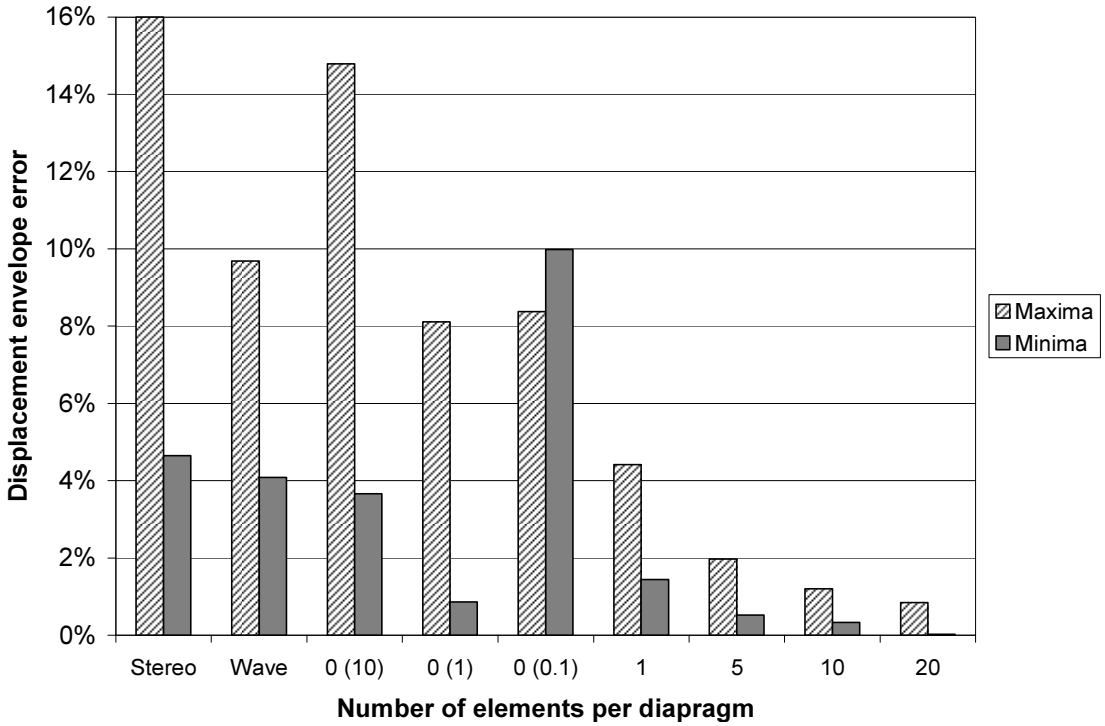

Figure 11: Displacement envelope error of building 2 (values of γ in parentheses)

A number of trends can be observed in the figure.

1. For the zero node diaphragms, the results from γ = 1 are the closest. However, as later sections show, this is not a consistent result.
2. Increasing the number of elements in the diaphragm increases the accuracy significantly.
3. The results from stereo mechanics are less accurate than that from the instant wave method.
4. Error from the 20 element diaphragm case is less than 1 %.

Due to the forth result and the long computational time of the 100 element diaphragms, the 20 element case is adopted as the accurate solution for all subsequent models. Five seconds of excitation required 17 days computation for the 100 element case.

Figure 12 shows the force profile for the third collision. As seen in the figure, the 5 and 100 element cases both indicate a collision force of approximately 1350 kN. However, due to the shapes of the collision profiles for the 1 and 0 element cases, a specific force magnitude is

difficult to identify. While the peaks of each profile may seem a reasonable indicator, their accuracy depends on each system configuration. The collision force may also be calculated by Equation 14 where pre-collision velocities are obtained from outputs of the corresponding analysis (Table 1). Inspection of these values indicates that the use of Equation 14 is sufficient and easier than trying to determine a force from the collision element for n = 1 or less.

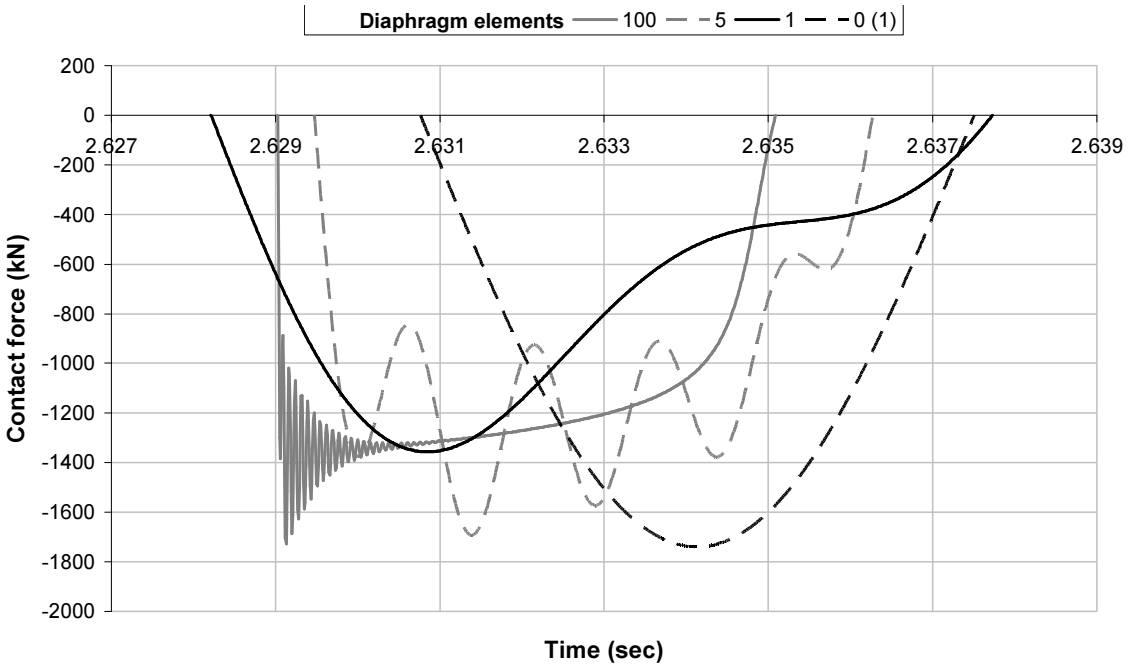

Figure 12: Collision 3 contact force

Case	Force (kN)	% Diff	Case	Force (kN)	% Diff
Stereo mechanics	1307	-1.5%	1	1330	0.2%
Instant wave	1323	-0.3%	5	1314	-1.0%
0(10)	1316	-0.8%	10	1319	-0.6%
0(1)	1283	-3.3%	20	1328	0.1%
0(0.1)	1243	-6.3%	100	1327	0.0%

Table 1: Collision force of collision 3 calculated by Equation 14

The shape of the collision force is essentially the same for a given number of elements. Figure 13 shows three collisions normalized by their maximum force. The normalized theoretical values are also displayed. The decay observed in the recorded force history is due to both the 5 % modal damping and the accelerations in each diaphragm at the time of collision. Note that accelerations predominantly oppose the current direction of motion. Refer to Figure 6a, if both diaphragms accelerations are opposing their respective velocities at the onset of collision, the relative velocity of particles distant from the collision interface will decrease with time. This lowers the internal stress in each diaphragm and consequently the collision force itself. Sufficiently high accelerations can cause collisions to stop before any natural collision period is reached. The damping generally extends the length of the collision. The initial oscillation at the beginning of the collision is due to the sudden change in stiffness of the collision element. Generally speaking the more elements there are in each diaphragm, the higher the frequency of these oscillations. Figure 13 shows that the collision profile is well characterized by wave theory.

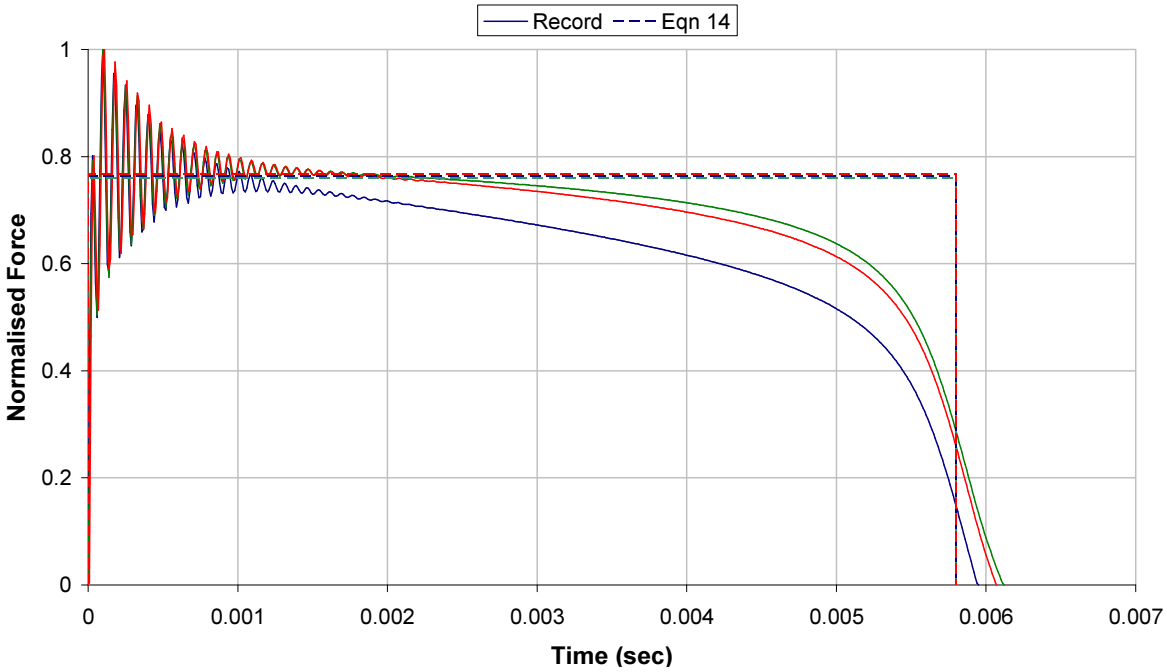

Figure 13: Normalized collision profiles for 100 element diaphragm

As the number of elements increases, the maximum time step required for convergence substantially drops. This is partly due to the modeling of the higher frequency modes, but primarily caused by the damping matrix. At higher modes, the 5 % uniform damping causes an energy imbalance in the terms of the equations of dynamic equilibrium. The only means of removing this error is to either use a smaller time step or reduce the level of damping. The maximum allowable time step was subsequently explored based on three criteria and presented in Table 2;

1. Energy loss over five seconds does not exceed 1 %;
2. Displacement envelopes do not differ more than 10 % from the accurate solution; and
3. The recorded final contact force can be quantified from its force profile and is within ± 100 kN for an accurate solution of 1000 kN.

Elements per diaphragm	**0 (γ = 1)**			**1**			**5**			**10**			**20**		
Criterion	*1*	*2*	*3*	*1*	*2*	*3*	*1*	*2*	*3*	*1*	*2*	*3*	*1*	*2*	*3*
Time step (sec)															
1×10^{-7}													✓	✓	✓
1×10^{-6}										✓	✓	✓	•	✓	✓
1×10^{-5}							✓	✓	✓	•	✓	✓	•	•	•
1×10^{-4}	✓	✓	•	✓	✓	•	•	✓	✓	•	•	•			
1×10^{-3}	•	✓	•	•	✓	•	•	•	•						
1×10^{-2}	•	•	•												

Table 2: Effect of number of nodes on time step

Grey fields indicate an accurate solution based on all three criteria while hashed fields indicate accurate displacement results. Note that the 0 and 1 element cases are exempted from the third criteria as the profiles can never be meaningfully quantified. Obviously, a large time step

is more desirable as it requires less computation time. The optimum solution is therefore to determine the lowest number of elements required to provide suitably accurate displacement and loading results.

4.2 Pounding of elasto plastic structures

Table 3 shows the parameters for two adjacent single storey elasto plastic structures separated by 5 mm. Building parameters were specifically chosen to amplify wave propagation effects via the considerations of Section 3.2. Figure 14 illustrates the building configuration.

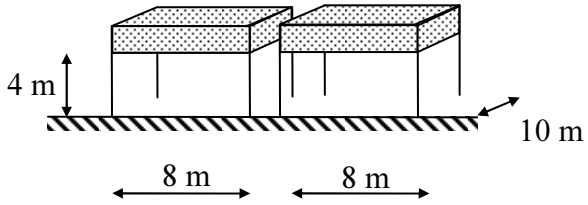

Figure 14 Single storey buildings subjected to pounding

Parameter	Building 1	Building 2	Ratio
Seismic weight	553 kN	414.5 kN	1.33
Interstorey stiffness	24254 kN/m	41764 kN/m	0.58
Diaphragm stiffness	1254200 kN/m	5016800 kN/m	0.25
Natural period	0.43 sec	0.28 sec	1.53
Natural col. period	0.013 sec	0.0058 sec	0.22
Stereo Mechanics α	0.429	0.572	-
Wave equation α	0.634	0.366	-
Yield load	100 kN	100 kN	1.0

Table 3: Elasto plastic building properties

The two buildings were subjected to three ten second excitations based on El Centro, Loma Prieta and Mexico City records. Each record was run with 0, 1, 2, 3, 4, 5 and 20 elements with $n = 0$ run for $\gamma = 10, 1, 0.1$. Figures 15 and 16 show the percentage difference in the maximum displacement envelope with respect to the 20 element case. Large errors are observed in the lower element models for building 2. Increasing the number of elements greatly reduces displacement error. Although $\gamma = 0.1$ appears to be the most accurate among the three zero element cases, the results for different γ should not be given much significance as other building configurations contradict this trend.

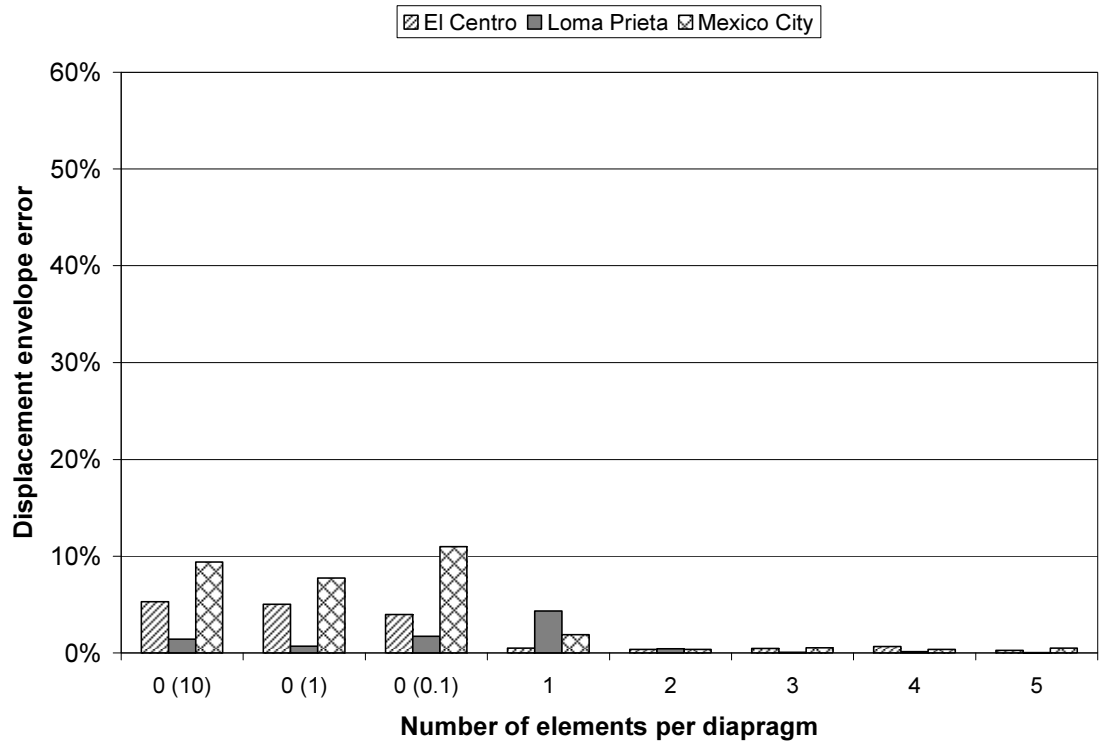

Figure 15: Building 1 displacement error

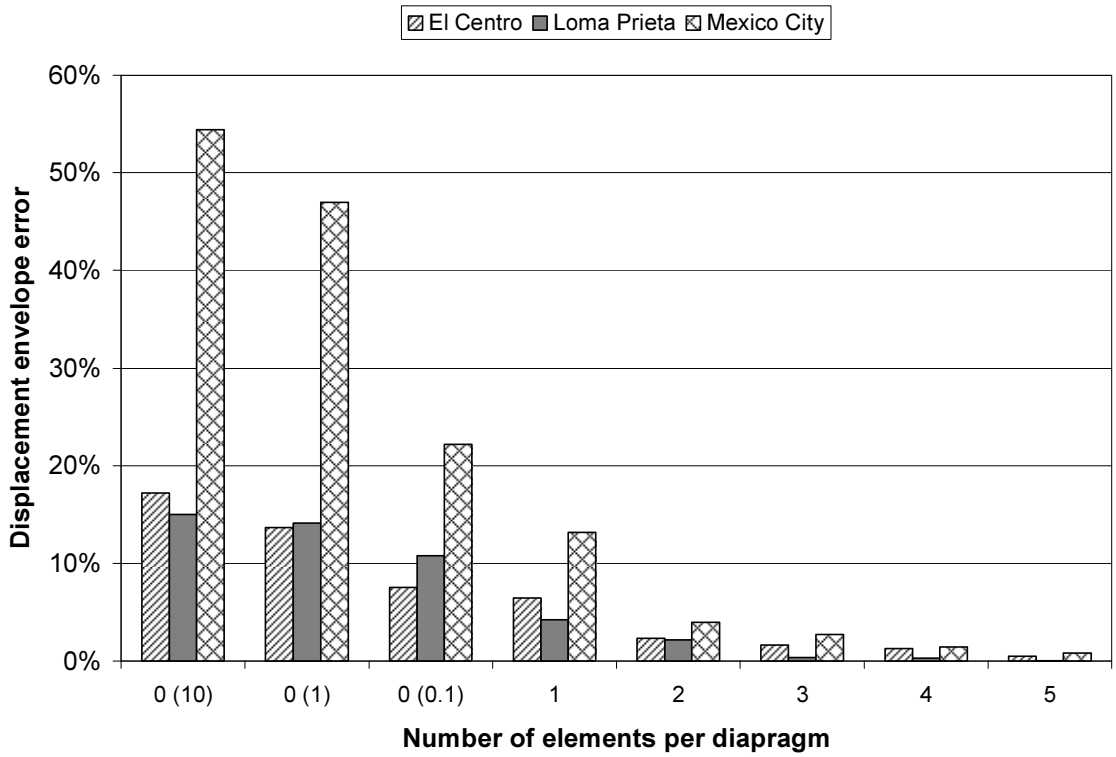

Figure 16 Building 2 displacement error

The 20 element case also provides reasonable contact force agreement with wave theory. Figure 17 shows the normalized force response for all three excitations, while Figure 18 compares the force magnitudes to those predicted by Equation 14. As shown in Table 3, the theoretical collision duration is 0.0058 seconds which is significantly less than most collision

durations seen in Figure 17. This is mainly due to secondary collisions which occur when the end of the distributed mass with the longer collision period expands faster than the final collision velocity of the other mass (refer to Figure 6b). Secondary collisions are necessarily smaller than the first collision and thus can be ignored if only the force magnitude is sought. The two curves that do finish close to 0.0058 seconds are actually very small collisions (with force less than 300 kN) and are likely more governed by their accelerations at the onset of collision.

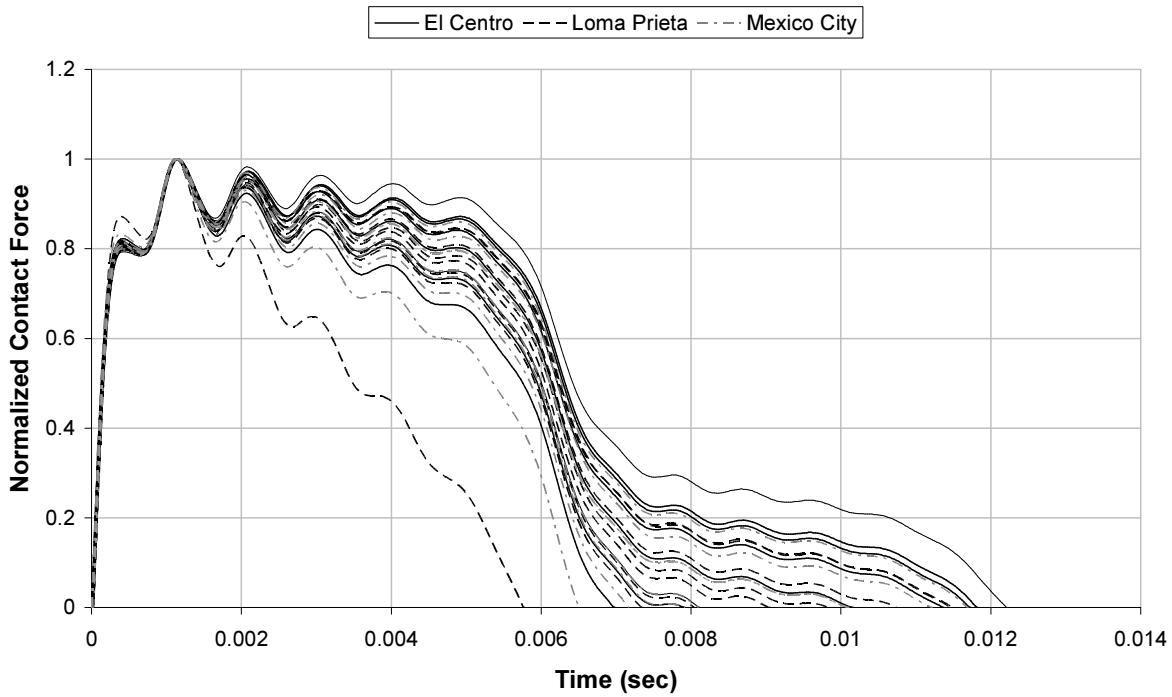

Figure 17: Collision profile

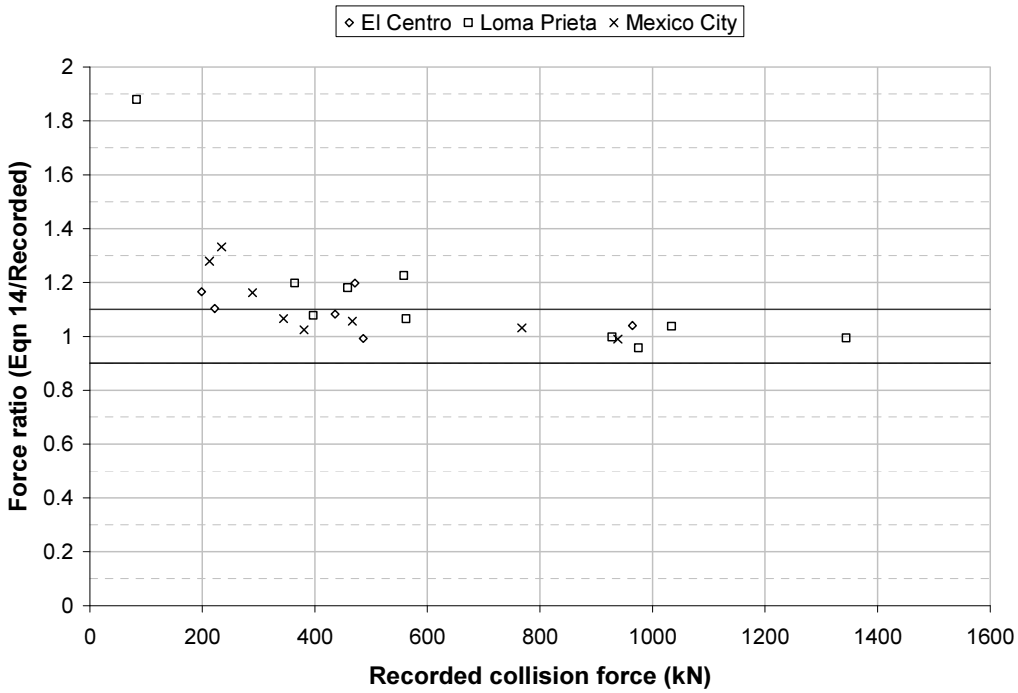

Figure 18: Accuracy of theoretical collision force (20 element diaphragms)

As can be seen in Figure 18, the predicted force magnitudes show varying accuracy. At very low magnitudes, the collision force is greatly overestimated, however the collision force becomes acceptably accurate for collisions greater than 800 kN. As interest is primarily directed to the critical cases, overestimation of the smaller collision forces is not considered to be a major problem.

4.3 Pounding of two storey elasto plastic structures

The final building configuration models two adjacent two storey buildings (Figure 19). Building data is presented in Table 4. The buildings are separated by 8 mm.

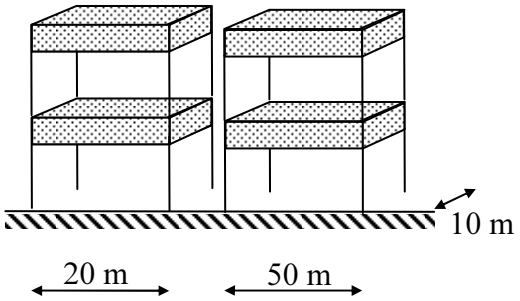

Figure 19: Two storey buildings subjected to pounding

	Building 1	**Building 2**	**Ratio**
Floor seismic weight	1600 kN	3000 kN	0.53
Interstorey stiffness	420000 kN/m	350000 kN/m	1.2
Diaphragm stiffness	1881300 kN/m	752520 kN/m	2.5
Natural period	0.2 sec	0.3 sec	0.67
Natural col. period	0.019 sec	0.04 sec	0.48
Stereo Mechanics α	0.652	0.348	-
Wave equation α	0.736	0.264	-
Yield load	2400 kN	1400 kN	1.71

Table 4: Building properties

Buildings are subjected to scaled versions of the same three excitations to induce different levels of inelastic behaviour. The El Centro record causes collisions to occur at both floor levels but induces very little inelastic excitation. Loma Prieta's second collision causes a large inelastic displacement and the Mexico city records excites moderate inelastic deformation.

Displacement results for the top level of the more flexible building 2 are presented in Figure 20. As noted in the previous section, no value of γ is consistently more accurate, but increasing the number of elements significantly reduces the displacement error. Normalized collision force profiles are presented in Figure 21. The profiles are again of similar form, with 30 % of contacts resulting in secondary collision. Note that every collision finishes by the longer natural collision period (refer Table 4). Seven collisions finish notably earlier than expected. These collisions are again dominated by the acceleration term. For example the Loma Prieta collision that concludes after 0.0169 seconds has a relative initial velocity of 0.21 m/s and a relative initial acceleration of -13.5 m/s^2. If a collision had element was not present, it would take 0.031 seconds for the two diaphragms to separate due to these kinematic conditions. As both the collision and the initial acceleration act to oppose the initial direction of

motion, the combined result is a much shorter collision, with an almost linear drop in collision force.

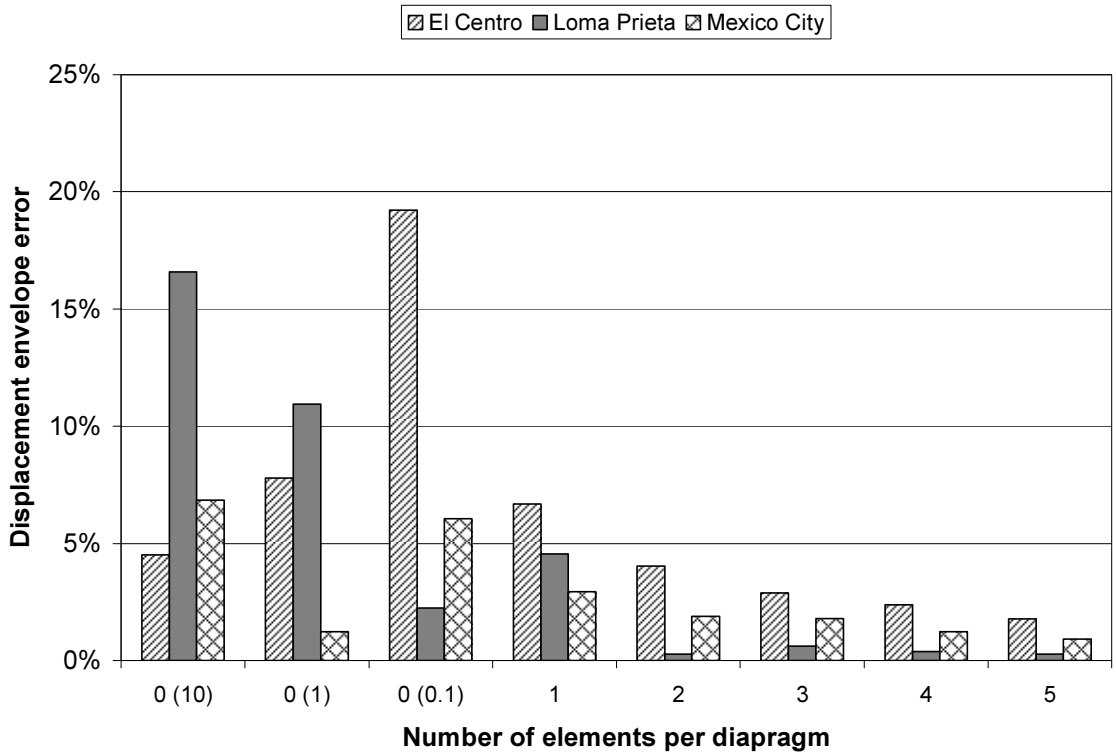

Figure 20: Building 2 level 2 displacement error

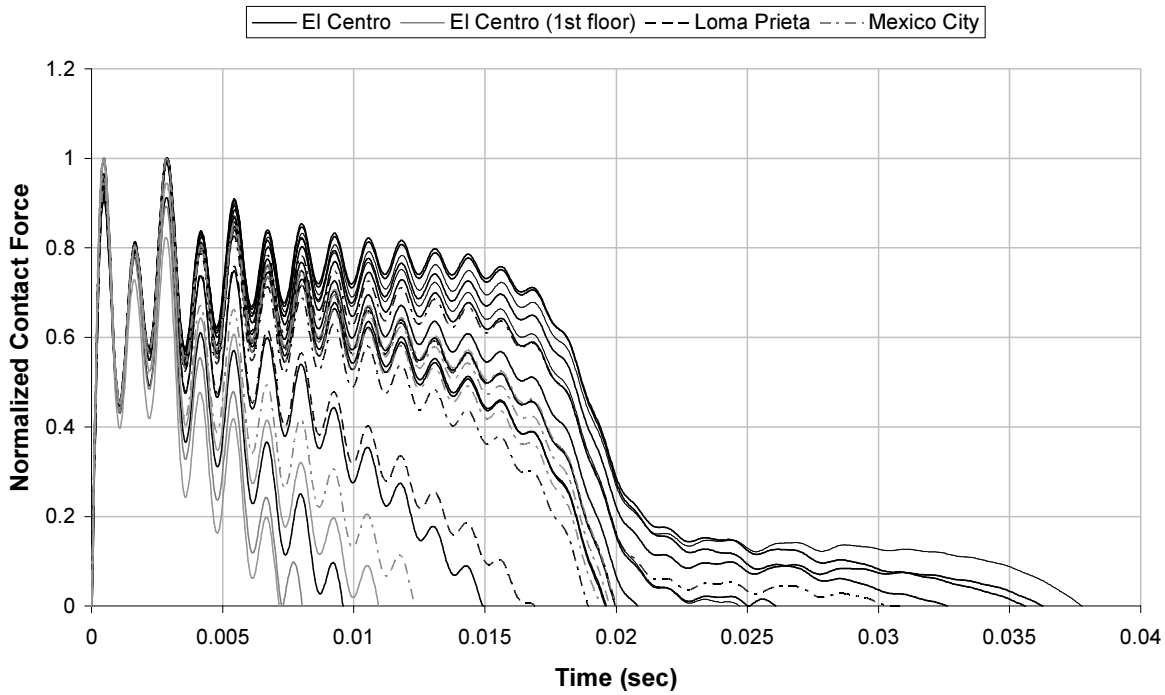

Figure 21: Collision force profiles for 20 element diaphragms

Figure 22 shows that the force magnitude is sufficiently accurately predicted when the force is greater than 1000 kN. Note this figure compares the theoretical contact force calcu-

lated based on Equation 14 only with that predicted by 20 element diaphragms. Figure 23 compares the theoretical contact force with all the numerical analyses for the El Centro record, including the first floor. If no collision was recorded, the force ratio is reported as zero. As the number of elements decreases, the force magnitude error increases. For large value contact forces, reasonable accuracy is found (within 10 %).

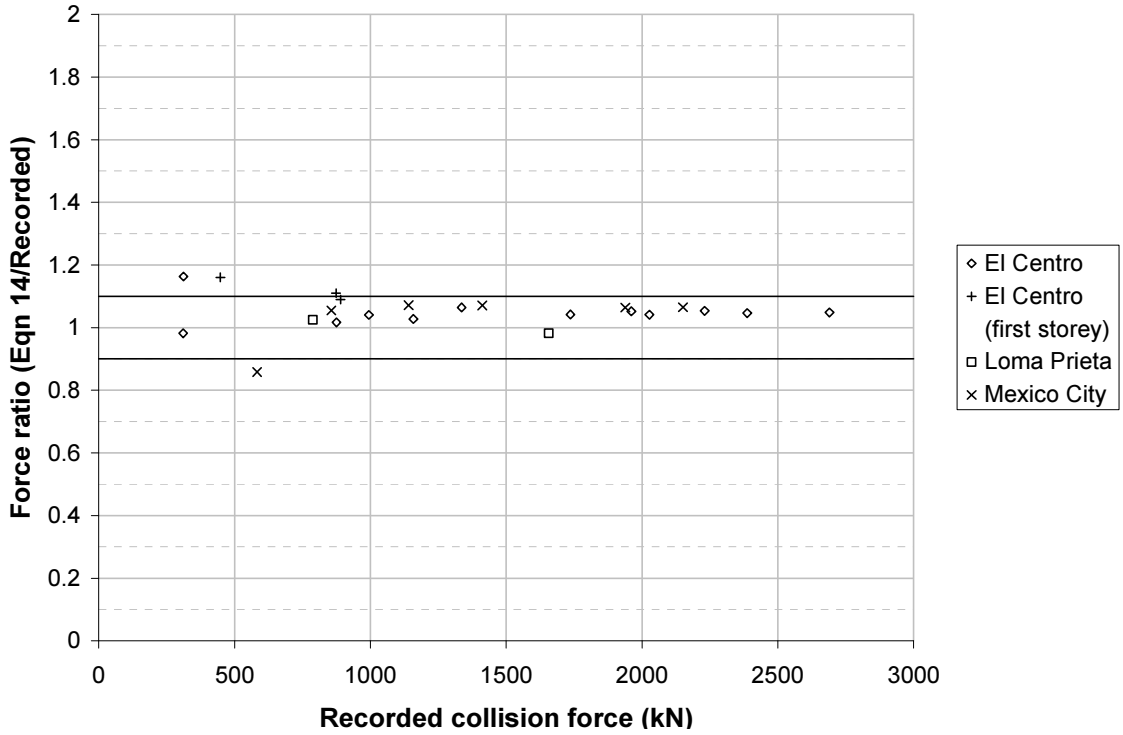

Figure 22: Accuracy of theoretically predicted collision force (20 element diaphragms)

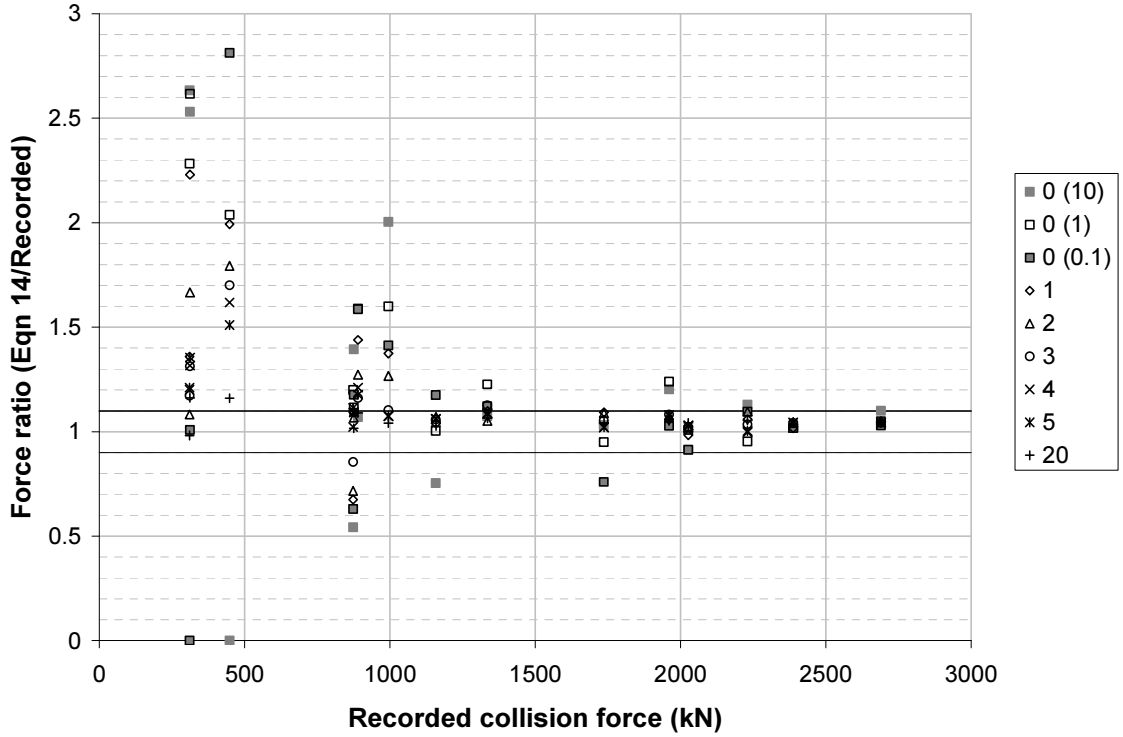

Figure 23: Effect of element number on accuracy of predicted force (El Centro record)

5 CONCLUSIONS

Based on the research presented herein and subject to the assumptions of Section 2.3, the following conclusions are drawn;

- Modeling floors as a single lumped mass is a physical misrepresentation of seismic pounding. Diaphragms are more appropriately modeled as distributed masses to account for the shock waves that travel through each mass during impact.
- An 'instant wave' model is developed based on classical wave theory. The instant wave model can be applied in a similar manner as the equations of stereo mechanics. The instant wave model predicts different post collision velocities than that of stereo mechanics and enables the prediction of impact forces. Two key parameters, α and collision period ratio, can also be used to qualitatively determine whether the effects of wave propagation will substantially change the response of a given building configuration.
- The post collision velocities of floors calculated by the instant wave method can substantially differ from that of stereo mechanics. However, this effect is less significant on the building displacement response.
- An impact force for the collision of two diaphragms is derived from the one dimensional wave equation and verified by numerical analysis. Collision force is found to be directly proportional to the relative velocity of the two diaphragms. The force is also affected by each diaphragm's mass and stiffness. The equation is found to slightly overestimate the collision force at low force magnitudes; but is reasonably accurate when the collision forces are moderate to high.
- All modeling based on the wave equation has been undertaken without any coefficient of restitution or collision specific damping. The uniform damping incorporated in all models provides some effective damping to the collision, but this parameter does not allow specific control of the collision damping itself. The suitability and effects of any collision specific damping requires further investigation.
- The zero and one element cases are found to have insufficient displacement accuracy. No optimum value of γ is found for the lumped mass (zero element) case. Accuracy is increased significantly by increasing the number of elements in each diaphragm. On the other hand, computational time increases if more elements are included to model each diaphragm.

Based on the above conclusions it is the authors' recommendation that pounding analyses be undertaken with at least three nodal masses connected by axial spring elements in each diaphragm. The contact element stiffness should be calculated with $\gamma = 1$ and the element stiffness of the stiffer diaphragm should be used in this calculation

6 ACKNOWLEDGEMENTS

The first author would like to acknowledge the Tertiary Education Commission and Beca, Carter, Hollings and Ferner Ltd for personal financial assistance to conduct this research.

REFERENCES

[1] G. Watanabe, K. Kawashima, Numerical simulation of pounding in bridge decks. *Proc. 13th World Conf. on Earthquake Engineering*, Paper no 884, Vancouver, Canada, 2004.

[2] V. Bertero, Observations on structural pounding. *The Mexico Earthquakes – 1985* p. 264 – 268. Mexico City, Mexico, 1986.

[3] S. Anagnostopoulos, Pounding of buildings in series during earthquakes. *Earthquake Engineering and Structural Dynamics*, **16**(3), p. 443 – 456, 1988.

[4] B. Maison and K. Kasai, Dynamics of poundings when two buildings collide. *Earthquake Engineering and Structural Dynamics*, **21**(9), p. 771 – 786, 1992.

[5] R. Davis, Pounding of buildings modelled by an impact oscillator. *Earthquake Engineering & Structural Dynamics*, **21**(3), p. 253-274, 1992.

[6] S. Muthukumar. and R. Desroches, Evaluation of Impact Models for Seismic Pounding, *13 WCEE: 13th World Conference on Earthquake Engineering Conference Proceedings*. Venue West Conference Services Ltd , Suite 645 - The Landing, 375 Water Street, Vancouver, B.C , V6B 5C6, Canada, 2004

[7] Jankowski, R., Non-linear viscoelastic modelling of earthquake-induced structural pounding. *Earthquake Engineering & Structural Dynamics*, **34**(6), p. 595-611, 2005.

[8] Goldsmith, W., *Impact: the theory and physical behaviour of colliding solids*., London, E. Arnold. 379, 1960.

[9] Athanassiadou, C. J., G. G. Penelis, et al, Seismic response of adjacent buildings with similar or different dynamic characteristics. *Earthquake Spectra* **10**(2): 293-317.1994

[10] Anagnostopoulos, S. A., Equivalent viscous damping for modeling inelastic impacts in earthquake pounding problems. *Earthquake Engineering & Structural Dynamics* **33**(8), p.897-902. 2004

[11] Jankowski, R., Non-linear viscoelastic modelling of earthquake-induced structural pounding. *Earthquake Engineering & Structural Dynamics* **34**(6): 595-611. 2005

[12] Chopra, A. K., *Dynamics of Structures: Theory and Applications to Earthquake Engineering*. New Jersey, Prentice Hall. 2007

[13] Carr, A. J. *Volume 2: User manual for the 2 Dimensional Version Ruaumoko 2D*. Christchurch, University of Canterbury. 2007